Nanomechanical probing of layered nanoscale polymer films with atomic force microscopy

A. Kovalev
Metal-Polymer Institute, National Academy of Sciences, 246050 Gomel, Belarus
H. Shulha and M. Lemieux
Department of Materials Science & Engineering, Iowa State University, Ames, Iowa 50011
N. Myshkin
Metal-Polymer Institute, National Academy of Sciences, 246050 Gomel, Belarus
V.V. Tsukruk[a)]
Department of Materials Science & Engineering, Iowa State University, Ames, Iowa 50011

(Received 2 August 2003; accepted 9 October 2003)

The approach developed for the microindentation of layered elastic solids was adapted to analyze atomic force microscopy probing of ultrathin (1–100 nm-thick) polymer films on a solid substrate. The model for analyzing microindentation of layered solids was extended to construct two- and tri-step graded functions with the transition zones accounting for a variable gradient between layers. This "graded" approach offered a transparent consideration of the gradient of the mechanical properties between layers. Several examples of recent applications of this model to nanoscale polymer layers were presented. We considered polymer layers with elastic moduli ranging from 0.05 to 3000 MPa with different architecture in a dry state and in a solvated state. The most sophisticated case of a tri-layered polymer film with thickness of 20–50 nm was also successfully treated within this approach. In all cases, a complex shape of corresponding loading curves and elastic modulus depth profiles obtained from experimental data were fitted by the graded functions with nanomechanical parameters (elastic moduli and transition zone widths) close to independently determined microstructural parameters (thickness and composition of layers) of the layered materials.

I. INTRODUCTION

The ability to probe surface mechanical properties with nanometer-scale lateral and vertical resolutions is critical for many emerging applications involving nanoscale (1–100 nm) compliant coatings for microelectromechanical and microfluidic devices where nanoscale details of surface deformations and shearing play a critical role in overall performance.[1–6] Usually, a nanomechanical probing experiment exploits either atomic force microscopy (AFM) or microindentation techniques.[7,8] The utilization of conventional microindentation techniques for systems consisting of highly compliant (elastic modulus ranging below 3000 MPa) and ultrathin (thickness below 100 nm) polymer coatings faces critical challenges associated with uncontrolled initial indentation, which can easily span the entire thickness of compliant nanoscale coatings and limits lateral resolution to hundreds of nanometers. Despite numerous technical issues associated with the AFM nanoprobing (e.g., nonaxial loading, jump-into contact, high local pressure, and topographical contributions), a number of successful applications have recently been demonstrated including nanomechanical probing of spin-coated and cast polymer films, organic lubricants, self-assembled monolayers, polymer brushes, biological tissues, and individual tethered macromolecules.[9–17] Absolute values of the elastic modulus have been measured for polymer surfaces in the range from 0.01 MPa to 30,000 MPa. These measurements were conducted in a wide range of temperatures and probing frequencies, for compliant films with thickness down to 2 nm, and with vertical and lateral resolution as low as 1–2 and 5–10 nm, respectively. Elastic moduli (loss and storage), surface glass transition temperatures, and relaxation times all have been obtained with reasonable confidence by applying direct dc or ac force–distance measurements and/or cantilever modulated (vertically as well as laterally) modes.[18–20]

[a)]Address all correspondence to this author.
e-mail: vladimir@iastate.edu

Spatial (concurrent vertical and lateral) resolution on a nanometer scale unachievable by any other probing technique makes AFM nanomechancial probing a unique experimental tool. We believe that a further expansion of the AFM-based probing of ultrathin (below 10 nm) polymer films in a contact mode regime will rely on solving several fundamental issues including the evaluation of substrate effect and the elastic response for multilayered coatings. In this communication, we present our work to adapt known approaches developed for the analysis of microindentation experiments of the elastic layered solids to AFM experiments. The results of corresponding AFM probing of several types of nanoscale polymeric coatings on solid substrates representing two- and trilayered structures are reported and discussed.

A. General contact mechanics background

General relationships between the normal load and the elastic indentation are suggested in classical Hertzian and Sneddon theories, with more complex cases analyzed with the Johnson–Kendal–Roberts approach as described in original papers and books.[21–25] As considered, indentation depth is a function of the applied force (normal load) P, tip geometry (radius R or parabolic focus distance c), as well as the mechanical and the adhesion properties of the contacting bodies. The normal load for AFM nanomechanical probing experiments conducted as depicted in Fig. 1 is calculated as $P = k_n \cdot z_{defl}$, where k_n is the vertical spring constant of the cantilever deflected in vertical direction by z_{defl}. A nonaxial displacement of the AFM cantilevers caused by their tilted orientation does not usually exceed 5–10% and, thus, will be neglected here. The above mentioned R (or c) and k_n are initial system parameters, which must be measured and calibrated before the nanomechanical analysis. The Poisson ratio, ν, is used as well as a material parameter and is usually assumed to be known and taken as a bulk value with possible deviations playing a minor role as was already demonstrated for microindentation experiments.[19]

As suggested in recent contact mechanics studies, the most general relationship between indentation depth, h, and normal load, P, in the course of indentation experiment can be presented in the very general form as:[21–25]

$$P = ah^b \quad , \tag{1}$$

where a and b are specific, model-dependent geometrical parameters (e.g., $b = 3/2$ for both Hertzian and parabolic Sneddon's contacts).[24]

On the other hand, the Sneddon model suggests a specific and practical analytical relationship between the surface stiffness, dP/dh and Young's modulus, E', in the form

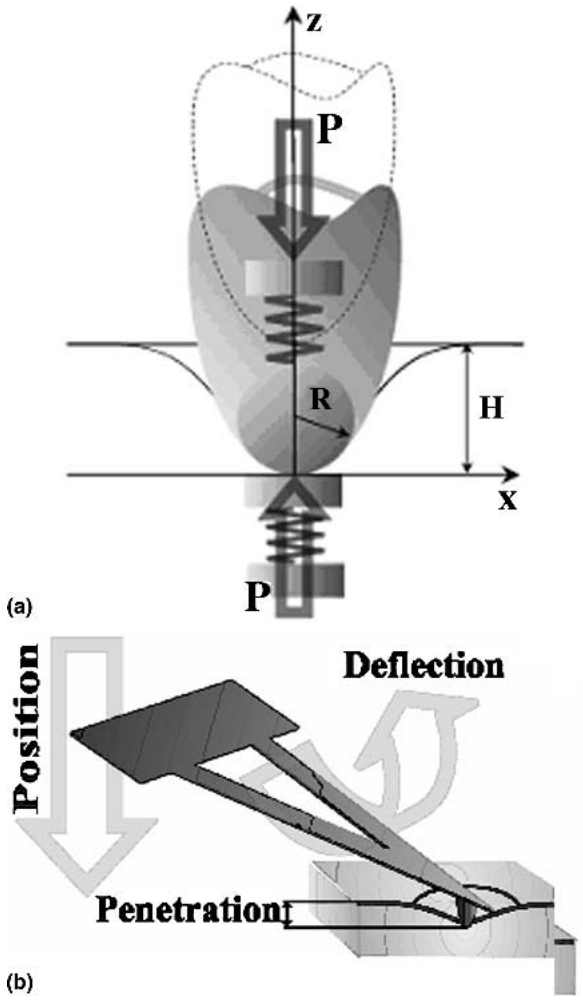

FIG. 1. (a) A two-spring model for the analysis of the loading curve for the parabolic tip–plane surface contact. (b) AFM cantilever deflection and indentation in the course of force–distance measurements.

$$\frac{dP}{dh} = \frac{2\sqrt{A}}{\sqrt{\pi}} E' \quad , \tag{2}$$

where E' is the composite modulus, and E_1 and E_2 are the elastic moduli of a surface and an indentor (tip). As known, the composite elastic modulus is defined as follows[25]

$$\frac{1}{E'} = \frac{1-\upsilon_1^2}{E_1} + \frac{1-\upsilon_2^2}{E_2} \quad . \tag{3}$$

From dP/dh dependence obtained from microindentation experiment and the calculated/measured contact area variation for a specific shape of the indentor (specific analytical expressions are suggested for circular, pyramidal, and parabolic shapes), one can evaluate an absolute value of the elastic modulus. For a routine estimation of the elastic modulus value for small indentation depths,

the Hertzian model of a sphere-plane contact type is applied. For larger indentations, the Sneddon model with a parabolic tip is usually exploited. The tip shape in the Sneddon model is described with equation $z = c \cdot x^2$, where c is a parabolic focus. This equation is very similar to the Hertzian equation but does not contain maximum indentation depth limitation.

B. Contact mechanics of layered elastic solids

There are several methods for the evaluation of the elastic modulus of thin films on solid substrates which include microindentation and bending experiments.[26–28] As suggested in these approaches, the compression of the layered elastic solids (e.g., a compliant film on a stiff substrate) results in concurrent deformations of two or more interfaces with local deformation depending on the mechanical properties of layers and a load transfer between adjacent layers (Fig. 2). Several different approaches have recently been developed to describe this phenomenon as will briefly be discussed below.

A double-layer model was proposed to describe deformational behavior within a modified Hertzian approximation.[29] The relation between a "modified" contact radius and Hertzian contact radius was suggested in the form

$$\frac{a}{a_{\text{hertz}}} = \left[\frac{J^{\frac{4}{3}} + 0.8 t/a_{\text{hertz}}}{\sqrt{1 + (0.8 t/a_{\text{hertz}})^2}} \right]^{1/4} , \qquad (4)$$

where a_{hertz} is the contact radius calculated from the Hertzian theory and J is the ratio of elastic moduli of two layers. Limitations of this theory included the consideration of only a compliant layer on a stiff surface and the absence of the criteria for the selection of any interlayer interaction. Our previous use of this approach demonstrated that some improvement of the fitting procedure can be obtained for polymer films on solid substrates.[30] However, for very thin films, this model usually overestimates indentation depth (see one representative example in Fig. 3).

A more sophisticated model, which considered the elastic deformation of the layered solids with a certain transfer of the mechanical load between adjacent layers, was proposed for the analysis of the microindentation data and was refined by several independent researchers.[31,32] A general key point of this approach was the suggestion to represent the composite compliance of two-layered solids (e.g., a film–substrate system) as a superposition of individual compliances in the form

$$\frac{1}{E'} = \frac{1}{E_f} \cdot (1 - e^{-a \cdot h/t}) + \frac{1}{E_s} \cdot (e^{-a \cdot h/t}) \quad , \qquad (5)$$

where E_f and E_s are elastic moduli of the film and the substrate, t is the total thickness of the film, h is the indentation depth, and α is a parameter defining contributions of different layers.

This representation is reminiscent of Eq. (3) for the composite modulus of two deformed solids in the mechanical contact. However, this approach introduces a new measure of a level of the transfer of the mechanical deformation between layers represented by a specially selected function: the transfer function, $e^{-\alpha h/t}$. This transfer function depends on total thickness of the layer, indentation depth, and the properties of the interlayer interactions as reflected by the parameter α. The transfer function for the elastic layered solid has an initial small value for very small, initial deformations ($h \ll t$) and increases for larger deformations ($h \leqslant t$).

The parameter α was initially suggested as an empirically determined parameter to be selected for each specific layered system. However, a clear physical meaning of this parameter was missing from the description proposed. Specific values of this parameter were experimentally determined and discussed for different pairs of

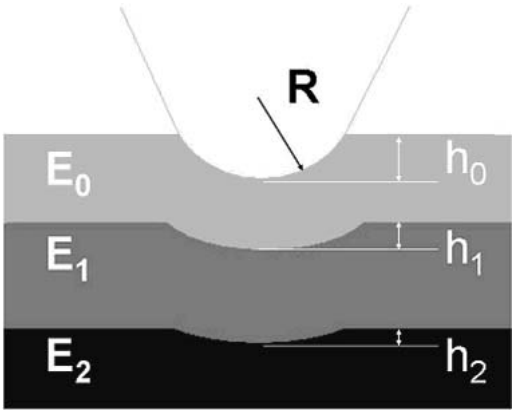

FIG. 2. Simultaneous deformation of several elastic layers for the layered solid and corresponding parameters of the tri-layered model as discussed in the text.

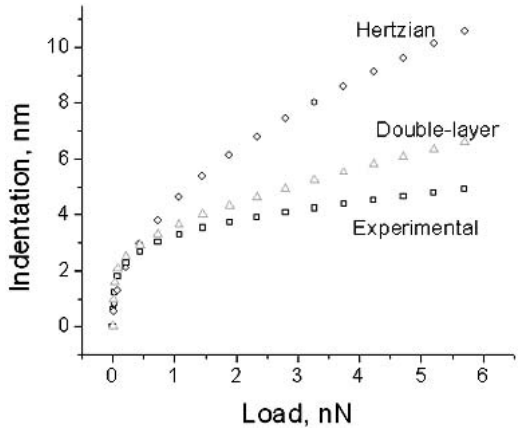

FIG. 3. An example of fitting of the loading curve for thin rubber layer on a solid substrate with Hertzian and double-layer models.[30]

solids, but clear interpretation and understanding of differences observed was not suggested.[33] Some modifications of this transfer function for different layered systems were suggested to improve experimental data fitting.[32,33]

Another approach starts from the representation of the nonuniform depth profile such as the one shown in Fig. 4 in an analytical form as a function of indentation depth h[34]

$$E' = E'_s + (E'_f - E'_s)\Phi(h) \quad , \tag{6}$$

where $\Phi(h)$ is the transition function describing a specific shape (gradient) of the depth profile of the elastic modulus (Fig. 4). In the framework of this approach, an indentor displacement and a stress propagation in a layered medium were analyzed by using the modified Sneddon solution for homogeneous solids. Careful contact mechanics analysis led to a complex expression for the transition function in the form[34]

$$\Phi = \frac{2}{\pi}\arctan\frac{1}{h} + \frac{1}{2\pi(1-\upsilon)}\left[(1-2\upsilon)\frac{1}{h}\ln(1+h^2) - \frac{h}{1+h^2}\right] \quad . \tag{7}$$

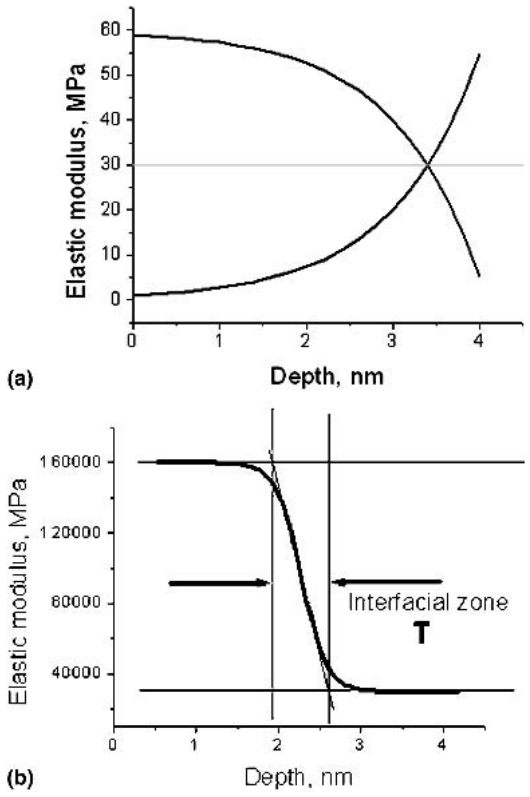

FIG. 4. (a) Examples of exponential functions used to describe gradient of the elastic properties. (b) The visualization of the depth profile for a hypothetical stiff-compliant film with two different levels of the elastic moduli (E_0 = 160,000 MPa and E_1 = 30,000 MPa). The interfacial zone, T, is defined for this profile as discussed in the text.

Considering that such a complex function is cumbersome in routine data analysis, alternative simpler models were suggested and used for the analysis of experimental data. For instance, a simple linear transition function was proposed:[35]

$$\Phi = E_f - (E_s - E_f)h \quad , \tag{8}$$

along with a more complex but still solvable exponential form[36–38]:

$$\Phi = e^{-ah} \quad . \tag{9}$$

These approaches provided a good analysis tool for a variety of specific cases of the layered solids as has recently been discussed in detail.[39] The comprehensive analysis conducted in this study demonstrated a reasonably good agreement of different approaches with the best fits obtained by using Eq. (7) and suggested some practical routines in implementing both experimental procedures and data treatment.

Below, we will show that a generalized approach that starts with a simple definition of the depth profile as a smooth function with gradual localized changes provides a means for the "visualization" of the transfer function and its concise interpretation for complex layered solids with two- and tri-layer architectures.

II. MODEL WITH VARIABLE ELASTIC MODULUS

A. Model description

Any variation of the elastic modulus along the vertical coordinate h (indentation depth) can be represented as a constant level superimposed with a combination of positive and negative local deviations

$$E'(h+\Delta h) = E'(h) + m * E'(h)\Delta h - nE'(h)\Delta h \quad . \tag{10}$$

This equation represents a change in the current value of the elastic modulus in the Δh range as the previous value, $E'(h)$, plus a combination of increasing $mE'(h)\Delta h$ and decreasing $nE'(h)\Delta h$ contributions, thus giving an expression for a local gradient as:

$$\frac{\Delta E'}{\Delta h} = (m-n)E'(h) \quad . \tag{11a}$$

In differential form and with $k = m - n$ representing a continuous balance of local deviations of the elastic modulus, this equation can be represented as:

$$\frac{dE'}{dh} = kE'(h) \quad . \tag{11b}$$

For a smooth monotonic function without singularities, it is natural to suggest that coefficient k depends on

the overall difference between moduli of two layers because larger local changes are generally required to accommodate larger overall difference in properties between adjacent layers. For the sake of simplicity, let's assume that coefficient k linearly depends on difference between a current modulus value and overall difference in elastic moduli of adjacent layers and α is a proportionality coefficient

$$k = \alpha[(E_1 - E_0) - E'(h)] \quad , \tag{12}$$

where E_0 and E_1 are two levels of the elastic modulus for a two-layered system (Fig. 4). The proportionality coefficient α can be either positive or negative depending on overall gradient of the elastic properties (compliant on stiff or stiff on compliant).

With this assumption, Eq. (11b) can be rewritten as:

$$\frac{dE'}{dh} = \{\alpha[(E_1 - E_0) - E']\}E' \quad . \tag{13}$$

If we set a new variable, $M = E_1 - E_o$, Eq. (13) is transformed to:

$$\frac{1}{M}\left(\frac{dE'}{E'} + \frac{dE'}{M - E'}\right) = \alpha dh, \left(\frac{dE'}{E'} + \frac{dE'}{M - E'}\right) = \alpha M dh \quad . \tag{14}$$

After integration we obtain:

$$\ln(E') - \ln(M - E') = \alpha M h + C \quad , \tag{15}$$

where C is the integration constant defined by the initial conditions.

If we define the "reference" depth h_o as a point where the modulus equals half of the difference between the two layers, $E'_0 = M/2$, then Eq. (15) is transformed to

$$C = \ln(E'_0) - \ln(M - E'_0) - \alpha M h_0 \quad . \tag{16}$$

After substitution, we obtain a new equation

$$\ln\left[\frac{E'(M - E'_0)}{(M - E')E'_0}\right] = \alpha M\,(h - h_0) \quad , \tag{17}$$

that can be converted to the final form after proper substitutions

$$E' = \frac{E_1 - E_0}{1 + \exp[-\alpha(E_1 - E_0)(h - h_0)]} \quad . \tag{18}$$

A selection of a sign for α depends on a gradient sign as was mentioned above. Let's introduce a new variable $\alpha' = \alpha E_0 h_0$. In this case we can rewrite Eq. (18) as

$$E' = \frac{E_1 - E_0}{1 + \exp[-\alpha'(E_1 - E_0)(h - h_0)/(E_0 h_0)]} \quad . \tag{19}$$

Overall, the depth profile of the elastic modulus for a two-layered system can be described as a superposition of the initial level and variable contribution for the two-layered system (19) as:

$$E(h) = E_0 + E'(h) \quad . \tag{20}$$

Modulus profile in this form can directly be used in Eq. (2) for fitting experimental data for the elastic response at a variable indentation depth.

The description proposed here is based on simple initial assumptions on the gradient properties of the layered systems and very basic arguments. It combines all major features suggested separately in several approaches discussed above and leads to a relatively simple Eq. (19) for the description of the elastic modulus gradient for two-layered systems. For the important case of a compliant film on a stiff substrate, only two unknown variables can be varied to fit experimental data (the elastic modulus of the top layer and parameter α') assuming that the elastic properties of the substrate are known. Usage of the proposed approach allows for the analysis of different layered structures. General profile of elastic modulus distribution as described by Eq. (19) is presented in Fig. 4. Two different levels of the elastic modulus are separated by a transition zone with a gradient of the elastic properties.

Equation (19) derived here independently from any previous approaches has, in fact, a form quite similar to Eq. (5) suggested before for microindentation experiments.[31] However, the shape of the transfer function suggested here is different and can be represented in the form $\exp[-\alpha' E' \Delta/(E_0 h_0)]$. This redefined transfer function takes into account not only overall indentation depth in correspondence to the overall thickness in the form $\Delta h = h - h_0$, where h_0 is the midpoint between two layers, but also the overall difference of the elastic moduli between layers (Fig. 4). Equation (19) in the current form allows for more detailed analysis of possible scenarios of intrafilm structures, contains transparent understanding of physical meaning of different parameters, and allows for the consideration of more complex cases of multilayered solids beyond two-layered systems. The developments will be discussed below along with limitations imposed by experimental routines.

B. Different layered systems

The variation of the elastic modulus in a wide range creates very different profiles including a virtually uniform distribution for a layered system with a small difference in elastic moduli (Fig. 5). It is worth noting that here and below in Figs. 6–8, the absolute values of the elastic modulus and the indentation depth were selected only for illustrative purposes, can be very different for different layered models, and are not to be used for the comparison between different layered models. The width

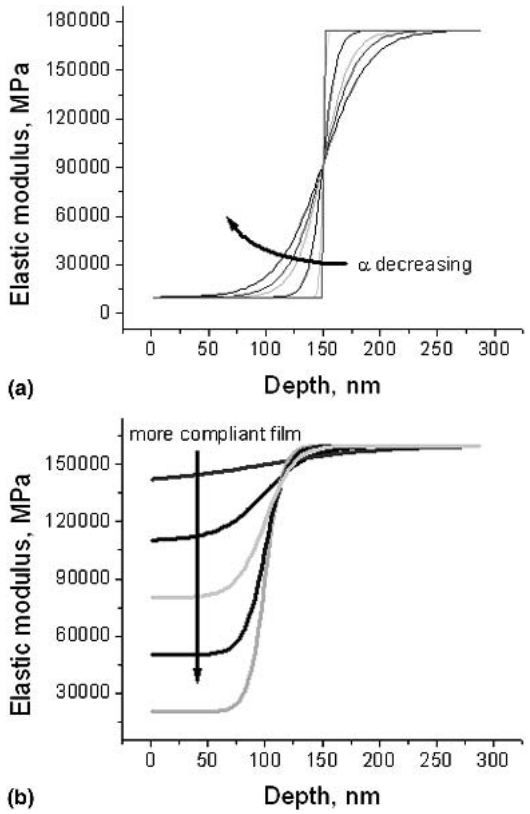

FIG. 5. (a) Influence of the transition parameter α on the overall shape of a hypothetical two-level depth profile of the selected elastic moduli (E_0 = 10,000 MPa and E_1 = 170,000 MPa). (b) Influence of the elastic modulus of the topmost layer on the total depth distribution of the elastic modulus of the two-layered solid (E_1 = 160,000 MPa).

of this transition zone between two layers is determined by the parameter α through the transition function. A high value of this parameter corresponds to a very sharp interfacial zone resulting in a step-like shape of $E'(h)$ (Fig. 5). Decreasing α-value results in a gradual broadening of the step-function with the formation of a virtually continuous gradient for a very low value of α (Fig. 5).

For practical purposes, instead of "nontransparent" parameters α, we introduce the thickness of the transition zone as the major fitting parameter as illustrated in Fig. 4. We calculate the "effective" thickness of the transition zone, T, as a distance between two points representing the intersections between two levels of elastic moduli and the slope to the fitting curve in the point where the value equals the average of the above-mentioned moduli. This parameter has direct physical meaning as a measure of the sharpness of the transition zone between layers (see Fig. 4 for the definition of the thickness of the transition zone). A reasonable physical value of this parameter and its correlation with expected or known structural gradients (e.g., controlled by processing, deposition, or synthetic routine) are important verifications of the concept and the fitting procedure as will be discussed below.

The advantages of the approach proposed is that it can be extended to more complicated cases of tri- (and more) layers by modifying Eq. (18) to include a recursive extension toward complex graded functions. For example, for the tri-layer structure, the model includes two independent values of the elastic modulus and the transition zone as fitting parameters assuming that the substrate properties are fixed (see Fig. 6). The corresponding complex but still analytically solvable expression can be derived from (18) as follows:

$$E' = E_0 + \frac{\left\{E_1 + \dfrac{E_2 - E_1}{1 + \exp[\alpha_1(E_2 - E_1)(h - h_0)]}\right\} - E_0}{1 + \exp\left[\alpha_2\left(\left\{E_1 + \dfrac{E_2 - E_1}{1 + \exp[\alpha_1(E_2 - E_1)(h - h_0)]}\right\} - E_0\right)(h - h_1)\right]}, \quad (21)$$

with E_0, E_1, and E_2 representing three levels of the elastic modulus for the tri-layered system (Fig. 6).

Using this expression, a tri-step graded function can be simulated to analyze the surface structure with a complex profile of stiff on compliant on stiff type (Fig. 6). By the variation of the transition zone gradient, this step-function can be converted from a sharp step-function to a smooth function with a minor depletion in the middle (Fig. 6). On the other hand, by changing the level of the elastic modulus for the intermediate layer, this function can be converted to the tri-layer function with ascending or descending elasticity (Figs. 6 and 7). Increasing of the thickness of the transition zone results in gradual transformation of the graded function to a smooth continuous gradient with virtually any shape (Fig. 7). And, unlike analytical functions with poorly defined boundary conditions used previously for the representation of the transition function, $\Phi(h)$, these graded functions contain clearly defined and separated physical parameters for controlling the level of the elastic modulus and gradient properties.

In the same way, it is possible to build even more complex layered systems such as the four-layer profile presented in Fig. 8. To show the depth behavior of the elastic response in this system, a set of the tri-layer film with decreasing elastic modulus located on a stiffer substrate was selected. The theoretical loading curve showed a non-monotonous behavior, which adequately reflected the complex elastic response of this system (Fig. 8). It is worth noting that in all these examples, both depth and elastic modulus values were selected for illustrative purposes only to reflect relative variations without any

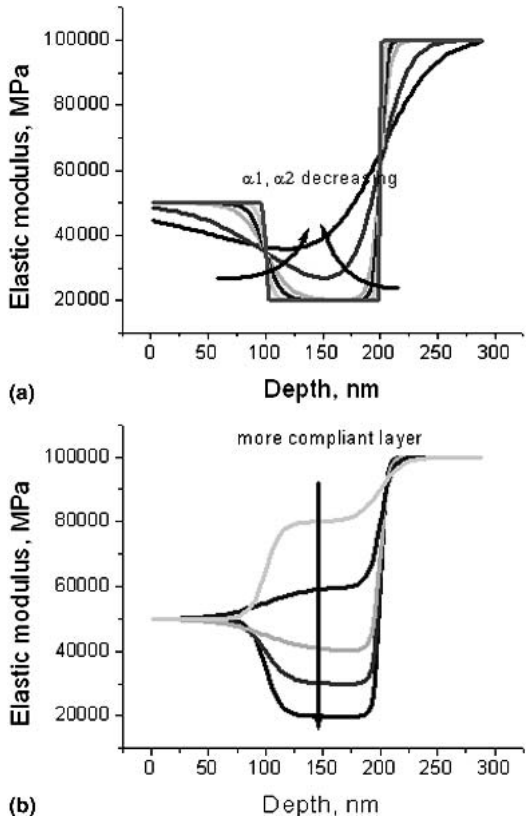

FIG. 6. (a) The variation of the transition parameter α in a hypothetical tri-layered system with selected values of elastic moduli (E_0 = 50,000 MPa, E_1 = 20,000 MPa, and E_2 = 100,000 MPa). Decreasing α results in the broadening of the transition zone and disappearance of the sharp steps. (b) Influence of the elastic modulus of the interlayer on the depth distribution of the elastic modulus of the tri-layer system presented above (E_o = 50,000 MPa and E_2 = 100,000 MPa).

intention to compare absolute values for different profiles.

Here, it is important to mention several other critical contributions that could affect force–distance data and are not accounted for in the model discussed here. First, strong adhesion between the AFM tip and surface can disturb the initial portion of loading curves and result in significant overestimation of the elastic modulus level at small indentation depth. We analyzed this contribution in our previous publication[40] and demonstrated significance of the adhesion hysteresis and initial non-zero contact area for very compliant polymeric materials with high adhesion (e.g., polar rubbery layers with the elastic modulus below 2 MPa and surface energy much higher than 20 mJ/m^2) in air. For these materials, an application of the Hertzian model resulted in manifold overestimation of the elastic modulus for small indentations. A complete Johnson–Roberts–Kendall model should be applied, which makes consideration significantly more complex and requires additional nontrivial measurements. However, for compliant materials with modest adhesion and higher stiffness, this overestimation is limited to a few initial data points and, thus, the approach discussed here can be applied. Second, a viscous contribution (time-dependent mechanical properties) can be critical in defining an overall shape of loading curves for viscoelastic polymeric materials. As we discussed earlier, this phenomenon would result in a concave shape of the force–distance curves, which, in fact, is sometimes observed.[30,41] This contribution can be treated by applying Johnson's recent development[42] as was discussed in separate publications.[30,43] For the analysis discussed here, we selected materials without significant viscous contributions (far from the glass-transition temperature where a contribution of the loss modulus does not exceed 10–20% of the elastic modulus value[44]) and probing frequencies in the range of minimal time-dependencies as was discussed earlier.[45] Third, the surface roughness of the layers studied here is extremely low, thus virtually eliminating any significant scattering in the first few data points observed for rough surfaces.[39] In fact, the surface microroughness does not exceed 0.2–0.5 nm for the layers studied here.

Finally, in all instances discussed here, we used a loading portion of the experimental force–distance data for

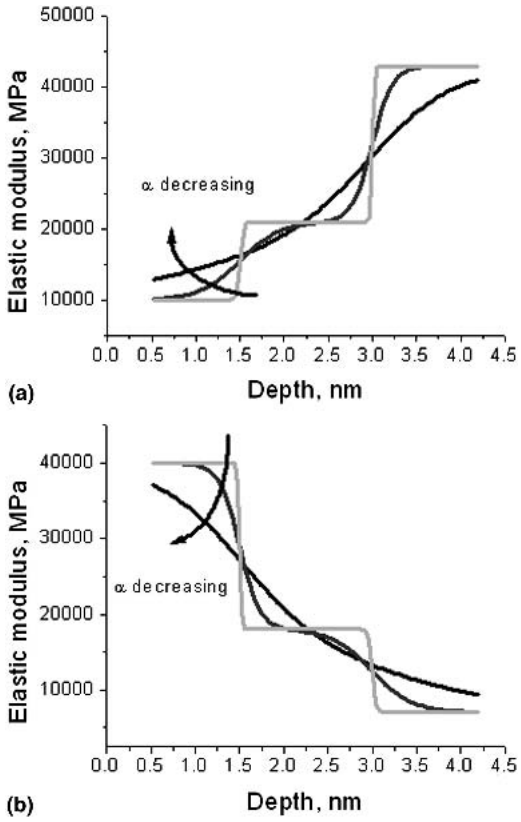

FIG. 7. Variable profiles of a hypothetical multilayered system with compliant-stiff-more stiff and stiff-compliant-more compliant layers and different transition parameters α: sharp steps, steps with interfacial zone, and continuous gradient ($E_0 < E_1 < E_2$ and $E_o > E_1 > E_2$).

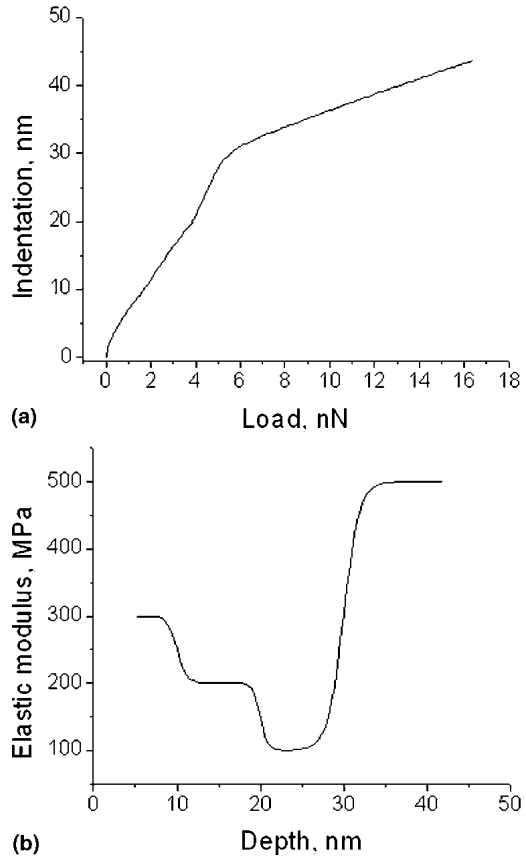

FIG. 8. A hypothetical model of a four layered coating in the case of stiff-compliant-more compliant-more stiff layering. (a) Loading curve, (b) The depth distribution of the elastic moduli with smooth transition zones for the same loading curve.

modulus estimation. This is justified by the fact that for purely elastic deformation, loading and unloading portions should be identical, which was indeed demonstrated for a number of compliant polymer surfaces.[45] The use of the unloading portion of force–distance curves is more complicated because some data points are affected by adhesive properties and the pull-off point cannot easily be defined. Below we will show several examples of unloading portions of the experimental data. In addition, in our evaluation of the elastic modulus for the topmost layer, as initial parameter for the input in fitting procedure, we used apparent value of the elastic modulus extrapolated to zero indentation depth. In many cases, the final value for the best fit was fairly close to this value.

III. ANALYSIS OF SELECTED EXPERIMENTAL DATA FOR LAYERED POLYMER FILMS

Experimental data for ultrathin, layered surface polymer coatings with different microstructures were obtained on Dimension 3000 and Multimode Nanoscope III (Digital Instruments, Santa Barbara, CA) atomic force microscopes. Experiments were done in a dry environment and in a fluid according to the experimental procedures described elsewhere.[41,46] Spring constants were selected in the range from 0.06 to 10 N/m depending on sample elasticity and were measured according to described technique.[47] Tip radius was measured with a gold nanoparticle reference standard.[48] Experimental force–distance data (cantilever deflection versus piezoelement displacement) collected in the force–volume mode were processed by *MManalysis* software package developed in our laboratory with an added option for the multilayered analysis.[49]

A. Two-layered system: Polymer brushes in air

Polymer brush layers are composed of macromolecules chemically grafted to a solid silicon substrate through a mediating functionalized self-assembled monolayer (Fig. 9).[50] In the case considered here, a binary polymer brush layer was prepared from rubbery poly(methyl acrylate) (PMA) and glassy poly(styrene-co-2,3,4,5,6-pentafluorostyrene) (PSF), both with high molecular weight, and was grafted to a silicon wafer by the "grafting from" approach as described elsewhere.[51] Independent measurements of these layers with ellipsometry and AFM scratch test gave a total thickness of the dry polymer layer of 50 nm with the rubbery phase having an overall thickness of about 5 nm.[51] An array of force–distance curves was collected for the surface areas of 2×2 μm. Surface topographical images were obtained before and after the experiments to confirm that deformations were elastic.

As an example, the average loading run of the force–distance curves obtained by averaging over 20 individual measurements over rubbery PMA phase within binary brush layer is presented in Fig. 9. Averaging was done to reduce the effect of noise that usually creates deviations of about 0.2–0.5 nm. All individual force–distance curves were similar to each other as demonstrated in Fig. 9. The averaging procedure produced a consistent shape but with much lower noise level and much better defined minimum point. The unloading portion of the force–distance curve closely followed the loading run for the large range of displacements except some data points affected by the presence of adhesive forces.

Due to the fact that the compliant polymer brush layer was deposited on a stiff silicon substrate, the force–distance curve displayed different slopes for small and large indentations. Accordingly, the shape of the loading curve deviates from the usual Hertzian behavior. Fitting with standard Sneddon model gives much larger indentations then observed in actual experiment due to the limitations imposed by the underlying stiff substrate (Fig. 9). However, an excellent fit was obtained with our approach using a high elastic modulus value, such as one

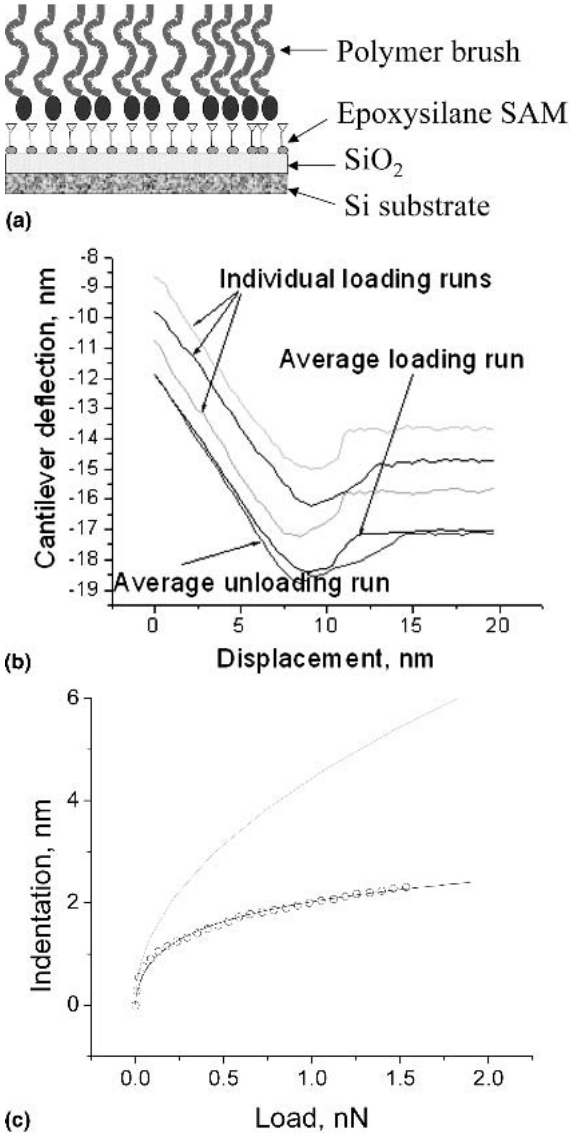

FIG. 9. (a) A general sketch of polymer brush layer with polymer chains tethered to the solid substrate via self-assembled monolayer.[51] (b) Experimental individual force–distance curves obtained for the dry PMA (compliant) phase on stiffer surface in binary brush layer[52] (loading runs are offset for clarity), the average loading run, and the average unloading run. (c) Fitting experimental loading curve (circles) by Hertzian model (dotted line) and the two-layered model (solid line) for the same value of the elastic modulus.

for the silicon substrate E_{substr} = 160,000 MPa (Fig. 9). Fitting parameters corresponded to the interfacial zone of 5-nm thickness and with the average value of compliant polymer layer of E_{layer} = 15 MPa. The latter value was close to that determined from depth profile and extrapolated to zero indentation depth. The values obtained here were close to ones known for the PMA polymer in the rubbery state deducted from measurements of homobrush layers and for interfacial zones of polymer brush layers grafted to organic self-assembled monolayer.[51,52]

However, significant variation (increase) of the elastic modulus of the polymer layers caused by the underlying stiff substrate was observed across the layer. Calculation of the depth profile from the loading run of force–distance curves proved that only initial, minor deformation not exceeding 2 nm was free from substrate influence or the presence of the glassy polymer component beneath (Fig. 10). For larger indentation, the apparent value of the elastic modulus increased gradually followed by dramatic increase for indentation depth larger than 4 nm. Overall fitting suggested that the elastic modulus profile could be represented by a two-step function with the intermediate thickness of the transition zone as presented in Fig. 10.

B. Tri-layered compliant system: Polymer brush layer in fluid

An example of the force–distance curve for the same binary polymer brush (PSF/PMA) placed in a good solvent for PMA (acetone) is presented in Fig. 11. Under this solvent, polymer chains were highly swollen and possessed very low elastic modulus as expected for

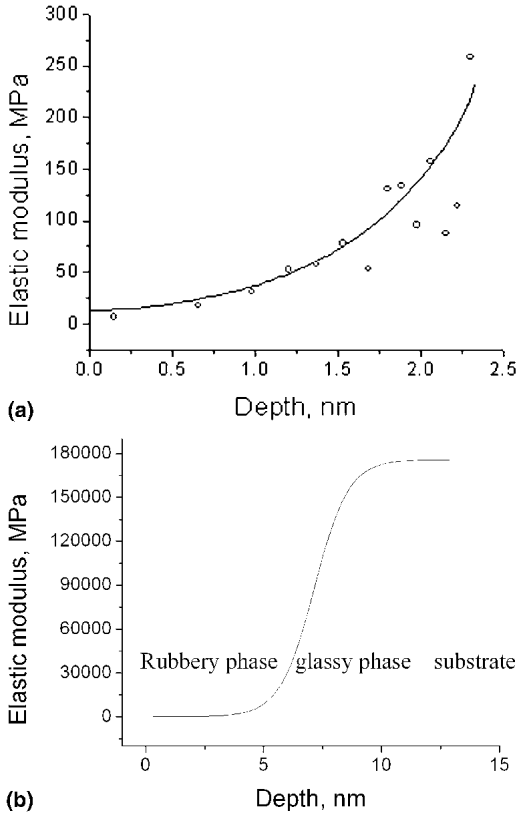

FIG. 10. (a) Fitting the experimental data on the depth distribution of the elastic moduli of dry polymer layer (circles) with the two-layered model (solid line). (b) Corresponding full-scale, two-layered depth distribution of the elastic modulus with clearly observed transition zone and suggested distribution of different polymer components.

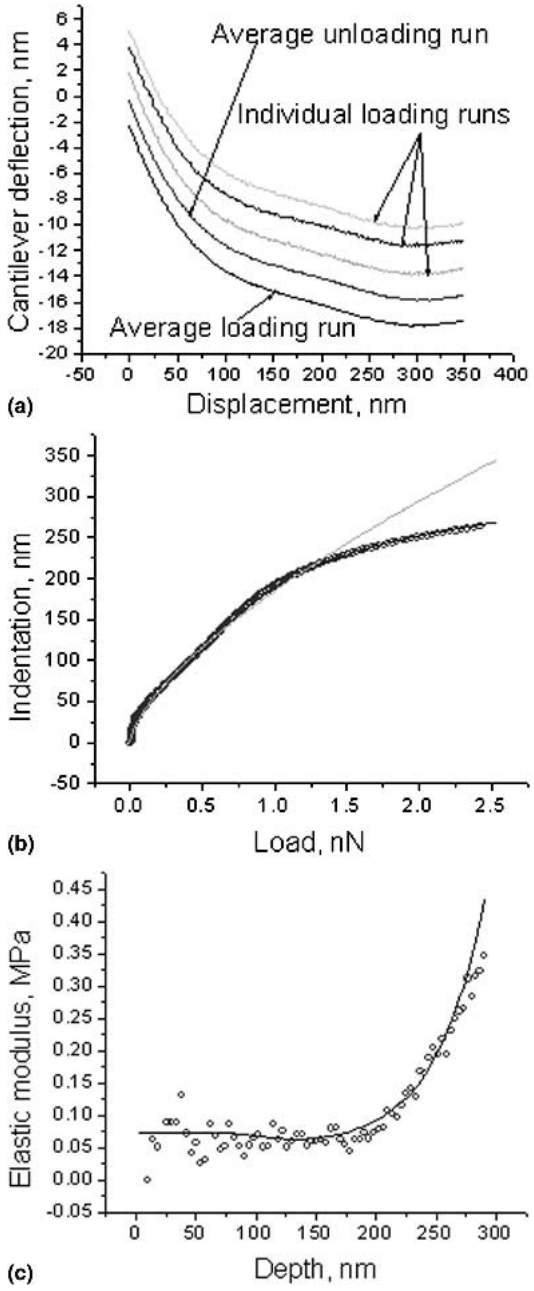

FIG. 11. (a) Experimental individual force–distance curves for the swollen polymer brush in solvent (loading runs, curves are offset for clarity), the average loading run, and the average unloading run (the average unloading curve is offset to avoid complete overlapping with the loading portion). (b) The experimental loading curve (circles), fitting with the tri-layered model (solid line, almost completely buried by experimental data points) and Hertzian model (dotted line). (c) Experimental depth distribution of the elastic modulus for the polymer brush layer (circles) and the best fitting with the tri-layered model (solid line) showing slight increase in the elastic modulus near the surface and sharp increase in proximity to a stiff substrate.

polymers in a good solvent.[52] Under these conditions, force–volume probing with very low normal forces (a spring constant of the cantilever was about 0.06 N/m) generated an array of force–distance curves with a complex shape showing three regions with different slopes. Accordingly, the loading curve with the indentation depth reaching 250 nm (the total thickness of the layer was about 300 nm as observed for scratched areas) displayed a complex shape, which deviated significantly from normal Hertzian behavior expected for a uniform elastic material (Fig. 11). Individual force–distance curves had similar shapes with higher level of noise removed by the averaging of a significant number of experimental curves.

Loading and unloading runs of the force–distance curves were virtually identical, and significant off-set was required to clearly show them on a plot (Fig. 11). The best fitting of the loading curve and the depth profile can be obtained by using a very low elastic modulus value of 0.07 MPa for initial deformations not exceeding 200 nm. This very compliant region is replaced with rising elastic resistance for larger indentation depth caused by the presence of the underlying solid substrate (Fig. 11). Slightly increased elastic modulus near the surface related to minor brush layering could be described by a tri-layered model reflecting the segregation of the tougher polymer near the surface. This higher elastic resistance for initial indentations was consistently observed for the majority of surface locations. Low values of the elastic modulus and the large thickness of the swollen polymer layer obtained from nanomechanical testing were close to that known for these systems from independent measurements with ellipsometry and for homobrush layers without second component.[52]

C. Tri-layered system: Grafted sandwich coating

Polymer "sandwich" system was prepared by grafting the rubber polymer interlayer of 10-nm thickness to functionalized self-assembled monolayer on a silicon wafer and capping this interlayer with a photopolymerized stiff polymer topmost layer with the thickness between 10–30 nm (Fig. 12).[53,54] This model represents a complex tri-layer system with elastic modulus changing from 2000 MPa for the topmost layer to 5–10 MPa for the rubbery interlayer and to 1000 MPa for underlying organic layer on 160,000 MPa silicon substrate as was independently measured for these materials. The elastic character of deformation was tested by zooming-out the surface area probed and observing absence of the indentation marks.

In fact, the force–distance curves collected on different surface locations demonstrated clearly a non-monotonic character with three different local slopes as is better visible in the average curve (Fig. 12). This non-monotonic character became more visible on the loading curve, which showed pronounced S-shaped behavior (Fig. 13). Attempts to fit the experimental data with

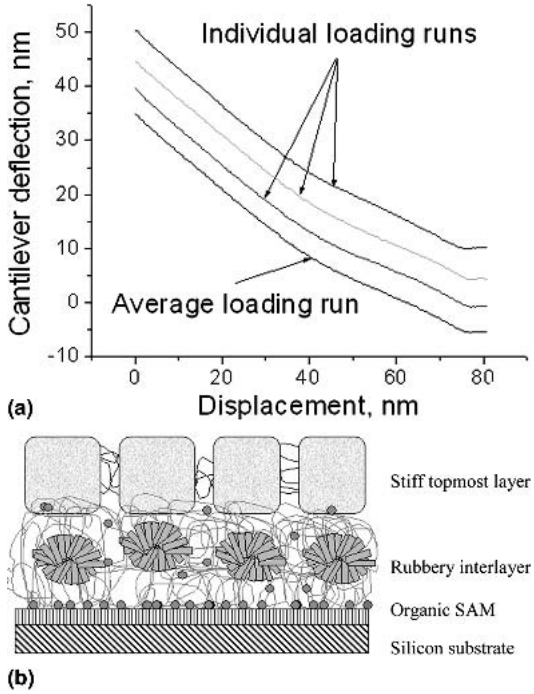

FIG. 12. (a) Experimental individual force–distance curves (loading runs, curves are offset for clarity) and the average loading run for this tri-layer film. (b) Sketch of the sandwich coating with stiff-compliant-stiff sequence of layers fabricated from grafted polymer layers of different types.[53]

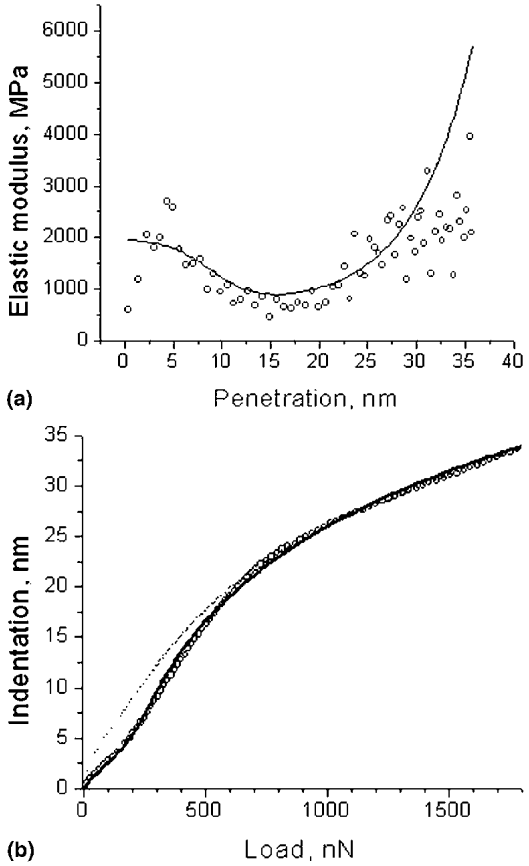

FIG. 13. (a) The depth distribution of the elastic modulus for the tri-layered polymer system from Fig. 12 (circles) and fitting with the tri-layer model (solid line). (b) Fitting of the experimental loading curve (circles) by the tri-layer model (solid black line, almost completely screened by experimental data points) and the best fit with Hertzian curve (dotted line).

Hertzian model failed: significant deviations were observed in the range of either low or high deformations depending on the selection of the elastic modulus value (Fig. 13). However, the experimental data could be fitted with a tri-layer model with modest gradient in the transition zones as demonstrated in Fig. 13. The best fit has been achieved with the tri-layer model composed of the topmost stiff layer 5-nm thick with the elastic modulus of 2000 MPa, a central interlayer 20-nm thick and the apparent elastic modulus of 800 MPa, and the solid substrate with the elastic modulus of 160,000 MPa (Fig. 13). The ultimate indentation of the tri-layer film was about 35 nm, which was close to the total thickness of the tri-layer film and indicated virtually complete compression under very high mechanical load. The thickness of the transition zone does not exceed 10 nm, which indicates modest gradient distribution between layers within the layered coatings.

Here, it is worth noting that the layer thickness obtained from the fitting procedure cannot be directly related to the known thickness of the independent layers but only to the corresponding deformation of these layers. It is also clear that the apparent elastic moduli for the elastic layers beneath the topmost layer are, in fact, not actual moduli of the layers but rather composite moduli presented by a linear combination of (3) or (5) types. This is also very true for the topmost layer, especially in the case of large deformations and relatively thin layers. Thus, for modest indentation depth when intermediate layers are accepting the mechanical load, one cannot expect the mechanical behavior associated with the elastic response of this layer but rather a more complex response involving weighted contributions from all deformed layers.

IV. CONCLUSIONS

In conclusion, the model proposed for analyzing microindentation of the layered solids was considered to construct two and tri-step graded functions with the transition zones reflecting variable gradient between layers. We modified this approach to include a transparent consideration of the gradient of the mechanical properties between layers with the transition zone concept. Several examples of a recent application of this model for the polymer brush surface layers in a dry state and in a swollen state (from 2- to 300-nm thick) and tri-layered

polymer films (15–50-nm thick) tethered to the solid substrate were presented to illustrate the fitting procedure. The range of tested thickness of the polymer layers was within typical molecular dimensions of the individual polymer chains which covered 2–100 nm for molecular weights of polymers within 5000–500,000, thus making this approach a truly nanoscale approach for probing of the nanomechanical properties on a molecular dimension scale. In both cases, complex shapes of the loading curves and the elastic modulus depth profiles obtained from experimental data were successfully fitted by the graded model with nanomechanical parameters (elastic moduli and transition zones) closely matching microstructural parameters of layered elastic materials known independently.

The approach proposed has limitations related to its eligibility only for purely elastic, completely reversible deformations without any contribution from plastic deformation, viscoelastic phenomenon, strong adhesion, and high friction. These contributions should be studied independently, and experimental probing conditions should properly be selected. The graded function approach also produces questionable results for extremely high difference in elastic moduli of the stiff substrate and the compliant layer generating too large thicknesses of the transition zone. The application of the routine discussed here to even simple two-layered materials is a subject of a number of "unwanted" contributions mentioned above, which can distort the results. The application to a tri-layer system is even more challenging and can produce unambiguous results only for proper combination of layer parameters. However, we believe that we clearly demonstrated that the approach proposed, if applied carefully and properly, can be used for the analysis of multilayered elastomeric materials with an appropriate thickness of different layers and an efficient load transfer between layers and substrates under conditions of purely elastic deformation.

ACKNOWLEDGMENTS

We acknowledge useful discussions with Dr. V.V. Gorbunov. This work was supported by The National Science Foundation (Grant Nos. CMS-0099868 and DMR-0308982) and through Grant No. M01-C03 from the United States Department of Commerce through the National Textile Center.

REFERENCES

1. R.S. Muller, in *Micro/Nanotribology and Its Applications*, edited by B. Bhushan (Kluwer Press, 1997), p. 579.
2. C.M. Mate and J. Wu, in *Microstructure and Microtribology of Polymer Surfaces*, edited by V.V. Tsukruk and K. Wahl (ACS Symposium Series **741,** 2000), p. 405.
3. *Micro/Nanotribology and Its Applications*, edited by B. Bhushan (Kluwer Press, 1997).
4. *Tribology Issues and Opportunities in MEMS*, edited by B. Bhushan (Kluwer Academic Press, 1998).
5. K. Komvopoulos, Wear **200,** 305 (1996).
6. E. Delamarche, A. Bernard, H. Schmid, B. Michel, and H. Biebuyck, Science **276,** 779 (1997).
7. X. Chen and J. Vlassak, J. Mater. Res. **16,** 2974 (2001).
8. V.V. Tsukruk, Adv. Mater. **13,** 95 (2001).
9. A. Matthews, R. Jones, and S. Dowey, Tribol. Lett. **11,** 103 (2001).
10. M.R. Vanlandingham, S.H. McKnight, G.R. Palmese, J.R. Ellings, X. Huang, T.A. Bogetti, R.F. Eduljee, and J.W. Gillespie, J. Adhes. **64,** 31 (1997).
11. V.N. Bliznyuk, M.P. Everson, and V.V. Tsukruk, J. Tribol. **120,** 489 (1998).
12. T. Kurokawa, J.P. Gong, and Y. Osada, Macromolecules **35,** 8161 (2002).
13. R. Domke and M. Radmacher, Langmuir **14,** 3320 (1998).
14. P. Lemoine and J. Mc Laughlin, Thin Solid Films **339,** 258 (1999).
15. P. Eaton, E.F. Fernandez, R.J. Ewen, T.G. Nevell, J.R. Smith, and J. Tsibouklis, Langmuir **18,** 10011 (2002).
16. V. Gorbunov, N. Fuchigami, M. Stone, M. Grace, and V.V. Tsukruk, Biomacromolecules **3,** 106 (2002).
17. V.V. Tsukruk, H. Shulha, and X. Zhai, Appl. Phys. Lett. **82,** 907 (2003).
18. B. Du, O. Tsui, Q. Zhang, and T. He, Langmuir **17,** 3286 (2001).
19. S.A. Asif Syed, K.J. Wahl, R.J. Colton, and O.L. Warren, J. Appl. Phys. **90,** 1192 (2001).
20. V.V. Tsukruk and Z. Huang, Polymer **41,** 5541 (2000).
21. W. Oliver and G. Pharr, J. Mater. Res. **7,** 1564 (1992).
22. I.N. Sneddon, Int. J. Eng. Sci. **3,** 47 (1965).
23. K.L. Johnson, K. Kendall, and A.D. Roberts, Proc. R. Soc. (London) A **324,** 301 (1971).
24. G.M. Pharr, W.C. Oliver, and F.B. Brotzen, J. Mater. Res. **7,** 613 (1992).
25. K.L. Johnson, *Contact Mechanics* (Cambridge University Press, Cambridge, 1985).
26. W.D. Nix, Metal. Trans. **20A,** 2217 (1989).
27. G.M. Pharr and W.C. Oliver, MRS Bull. **17,** 28 (1992).
28. J.S. Field and M.V. Swain, J. Mater. Res. **8,** 297 (1993).
29. A.P. Makushkin, Friction and Wear **11(3),** 423 (1990).
30. S.A. Chizhik, V.V. Gorbunov, I. Luzinov, N. Fuchigami, and V.V. Tsukruk, Macromol. Symp. **167,** 167 (2001).
31. M.F. Doerner and W.D. Nix, J. Mater. Res. **1,** 601 (1986).
32. R.B. King, Int. J. Solids Struct. **23,** 1657 (1987).
33. T. Sawa, Y. Akiyama, A. Shimamoto, and K. Tanaka, J. Mater. Res. **14,** 6 (1999).
34. H. Gao, C.H. Chiu, and J. Lee, Int. J. Solids Struct. **29,** 2471 (1992).
35. D. Pender, S. Thompson, N. Padture, A. Giannakopoulos, and S. Suresh, Acta Mater. **49,** 3263 (2001).
36. S. Suresh, Science **292,** 2447 (2001).
37. A.E. Giannakopoulos and S. Suresh, Int. J. Solid Struct. **34,** 2357 (1997).
38. A.E. Giannakopoulos and S. Suresh, Int. J. Solid Struct. **34,** 2393 (1997).
39. J. Mencik, D. Munz, E. Quandt, E.R. Weppelmann, and M.V. Swain, J. Mater. Res. **12,** 2475 (1997).
40. S.A. Chizhik, Z. Huang, V.V. Gorbunov, N.K. Myshkin, and V.V. Tsukruk, Langmuir **14,** 2606 (1998).
41. V.V. Tsukruk and V.V. Gorbunov, Probe Microscopy **3-4,** 241 (2002).
42. K.L. Johnson, in *Microstructure and Microtribology of Polymer Surfaces*, American Chemical Society Symposium Series **741,**

edited by V.V. Tsukruk and K. Wahl (Washington DC, 1998), p. 24.
43. H. Shulha, A. Kovalev, N. Myshkin, and V.V. Tsukruk (accepted).
44. J.J. Aklonis and W.J. MacKnight, *Introduction to Polymer Viscoelasticity* (John Wiley & Sons, New York, 1983).
45. V.V. Tsukruk, Z. Huang, S.A. Chizhik, and V.V. Gorbunov, J. Mater. Sci. **33,** 4905 (1998).
46. H. Shulha, X. Zhai, and V.V. Tsukruk, Macromolecules **36,** 2825 (2003).
47. J. Hazel and V.V. Tsukruk, Thin Solid Films **339,** 249 (1999).
48. M. Radmacher, R. Tillmann, and H. Gaub, Biophys. J. **64,** 735 (1993).
49. V.V. Tsukruk and V.V. Gorbunov, Microscopy Today **01-1,** 8 (2001).
50. I. Luzinov, D. Julthongpiput, A. Liebmann-Vinson, T. Cregger, M.D. Foster, and V.V. Tsukruk, Langmuir **16,** 504 (2000).
51. M. Lemieux, S. Minko, D. Usov, M. Stamm, H. Shulha, and V.V. Tsukruk, Langmuir **19,** 6126 (2003)
52. M. Lemieux, D. Usov, S. Minko, M. Stamm, and V.V. Tsukruk, Macromolecules **36,** 7244 (2003).
53. A. Sidorenko, H. Ahn, D. Kim, H. Yang, and V.V. Tsukruk, Wear **252,** 946 (2002).
54. V.V. Tsukruk, H. Ahn, D. Kim, and A. Sidorenko, Appl. Phys. Lett. **80,** 4825 (2002).